HHS Public Access

Author manuscript

Cancer Res. Author manuscript; available in PMC 2018 May 01.

Published in final edited form as:

Cancer Res. 2017 May 01; 77(9): 2292–2305. doi:10.1158/0008-5472.CAN-16-2832.

Local activation of p53 in the tumor microenvironment overcomes immune suppression and enhances antitumor immunity

Gang Guo[1], **Miao Yu**[1], **Wei Xiao**, **Esteban Celis**, and **Yan Cui**[*]

Cancer Immunology, Inflammation and Tolerance Program, Georgia Cancer Center, Department of Biochemistry & Molecular Biology, Medical College of Georgia, Augusta University, Augusta, GA 30912

Abstract

Mutations in tumor suppressor p53 remain a vital mechanism of tumor escape from apoptosis and senescence. Emerging evidence suggests that p53 dysfunction also fuels inflammation and supports tumor immune evasion, thereby serving as an immunological driver of tumorigenesis. Therefore, targeting p53 in the tumor microenvironment (TME) also represents an immunologically desirable strategy for reversing immunosuppression and enhancing antitumor immunity. Using a pharmacological p53 activator nutlin-3a, we show that local p53 activation in TME comprising overt tumor infiltrating leukocytes (TILeus) induces systemic antitumor immunity and tumor regression, but not in TME with scarce TILeus, such as B16 melanoma. Maneuvers that recruit leukocytes to TME, such as TLR3 ligand in B16 tumors, greatly enhanced nutlin-induced antitumor immunity and tumor control. Mechanistically, nutlin-3a-induced antitumor immunity was contingent on two non-redundant but immunologically synergistic p53-dependent processes: reversal of immunosuppression in TME and induction of tumor immunogenic cell death (ICD), leading to activation and expansion of polyfunctional CD8 CTLs and tumor regression. Our study demonstrates that unlike conventional tumoricidal therapies, which rely on effective p53 targeting in each tumor cell and often associate with systemic toxicity, this immune-based strategy requires only limited local p53 activation to alter the immune landscape of TME and subsequently amplify immune response to systemic antitumor immunity. Hence, targeting the p53 pathway in TME can be exploited to reverse immunosuppression and augment therapeutic benefits beyond tumoricidal effects to harness tumor-specific, durable, and systemic antitumor immunity with minimal toxicity.

Keywords

p53 activation; MDM2; immunosuppression; immunogenic cell death; anti-tumor immunity

[*]Corresponding author: Yan Cui, Cancer Immunology, Inflammation and Tolerance Program, Georgia Cancer Center, Department of Biochemistry & Molecular Biology, Medical College of Georgia, 1410 Laney Walker Blvd, CN-4120, Augusta, GA 30912, Phone: (706)-723-4153; Fax: (706)-721-4804; ycui@augusta.edu.

[1]These authors contributed equally to this work.

Introduction

Somatic mutations in tumor suppressor *p53* occur in more than 50% of human tumors (1–3). Most *p53* mutations are missense, causing inability to induce apoptosis and senescence, thereby promoting tumorigenesis. Recent observations from our laboratory and others suggest that *p53* dysfunction also fuels pro-tumor inflammation and is a gain-of-function immunological driver of tumorigenesis via skewing the immune landscape of the tumor microenvironment (TME) (4–9). Hence, targeting the p53 pathway represents a favorable immunological strategy besides its current application as a tumoricidal regimen (2,3,10,11). Recent remarkable success of immunotherapy underscores the pivotal role of reversing immunosuppression in the TME in augmenting T cell-mediated adaptive immunity for tumor control (12,13). Nonetheless, clinical results of systemic delivery of pharmacological p53 activators revealed high toxicity, especially hematologic toxicity that is detrimental to immunotherapy (14). Recent studies showed that targeted p53 activation/restoration via genetic approach activates NK cells and macrophages (15,16). It remains unknown and is imperative to investigate whether restricted p53 activation in the TME promotes sustained tumor-specific T cell activation

It is increasingly appreciated that activation of antitumor immunity is indispensable for the clinical benefits of radiotherapy and some types of chemotherapy (17–19). Mechanistically, those therapies promote antitumor immunity via eliciting tumor immunogenic cell death (ICD) (17,18,20). Chemotherapy and radiotherapy induce cell death via stress and DNA damage, which robustly activate p53. It is yet unexplored whether local p53 activation in the TME is necessary for ICD and/or sufficient to overcome the immunosuppressive TME promoting systemic antitumor immunity.

To this end, we treated murine tumors, EL4 and B16, with a pharmacological p53 activator nutlin-3a. Nutlin-3a, being tested in clinical trials for tumoricidal effects, activates p53 by inhibiting a natural p53 inhibitory molecule MDM2 (mouse double minute 2 homologue) (3,14,21). We observed that nutlin-3a induced p53-dependent ICD of EL4 and B16 tumors, but only resulted in activation of systemic antitumor immunity and tumor regression against immunogenic EL4 tumors, not non-immunogenic B16 tumors (22,23) following intratumoral injection. However, combination with other immunological maneuvers that enhanced the recruitment of tumor infiltrating leukocytes (TILeus) in the B16 TME, intratumoral injection of nutlin-3a induced significant antitumor immunity and improved tumor control. Mechanistic studies revealed that successful activation and amplification of systemic antitumor immunity by local p53 activation in the TME depend on two non-overlapping, but synergistic cellular processes: (a) p53-dependent conversion of immunosuppressive TME to immunostimulatory, and (b) p53-dependent induction of tumor ICD that further amplifies productive antitumor immunity.

Methods

Mice

Rag1^{null} (B6.129S7-*Rag1*^{tm1Mom}/J), *Trp53*^{null} (B6.129S2-*Trp53*^{tm1tyj}/J), *p53*^{loxP} (B6.129P2-*Trp53*^{tm1Brn}/J), *Vav-iCre* [B6.Cg-Tg(Vav1-icre)A2Kio/J], and *UBC-GFP*

[C57BL/6-Tg(UBC-GFP)30Scha/J] mice were purchased from the Jackson Laboratories (Bar Harbor, ME). *C57BL/6* mice were purchased from Charles River (Wilmington, MA). All mice were bred and kept under SPF conditions in the Georgia Cancer Center animal facility following protocols approved by the Institutional Animal Care and Use Committee.

Tumor inoculation and treatment

EL4 or B16F1 cells, purchased from ATCC (Manassas, VA), which were not independently authenticated in our laboratory, were maintained in DMEM (Invitrogen, Carlsbad, CA) supplemented with 10% FBS. The p53 function and intact p53 pathway of both cell lines were verified in our laboratory via real-time RT-PCR following nutlin-3a treatments. Either tumors were injected subcutaneously at 1 X 10^6/mouse in the right flank or 2 X 10^5/flank/injection for mouse receiving tumors in both flanks. Tumors were measured every other day and calculated as: volume = (length X width) X (length + width)/2. When tumors reached 100 – 300 mm^3, they received intratumoral injection of 100 μl of 20 μM nutlin-3a (Sigma, St. Louis) in PBS twice one-day apart or 50 μg/50 μl of poly-ICLC [poly-L-Lysine (Sigma) mixed with 2% carboxymethylcellulose and poly-IC (hmw, InvivoGen, San Diego)] in PBS followed by two nutlin-3a injections of 100 μl of 20 μM at one-day apart.

Flow cytometry analysis and MDSC purification

Antibodies for FACS were purchased from BD Biosciences (San Jose, CA), Biolegend (San Diego, CA) or eBioscience (San Diego, CA). Lymph nodes and tumors were processed as previously described (4). The effector T cell function was determined via intracellular cytokine staining following standard procedures (4). FACS acquisition was performed using BD^{TM}LSR II and analyzed using FlowJo (Tree Star Inc., Ashland, OR). Purification of TIL-MDSCs was carried out using FACSAria (BD Biosciences) to obtain viable cells, which were gated on DAPI negative populations, based on their CD11b, Gr-1, Ly6C, and Ly6G expression.

Histology and immunofluorescence (IF) of tumor specimens

Tumors were snap-froze in liquid N2. IF of the tumor sections were performed following standard protocols (4).

TUNEL staining

Novus (Littleton, CO) APO-BRDU (TUNEL) Apoptosis kit was used to examine dying cells with exposed or fragmented DNA ends as per manufacture's instruction. Briefly, tumor sections were first fixed with 4% formaldehyde, followed with proteinase K, and 3% H_2O_2 treatment. Exposed DNA ends were subsequently labeled with Br-dTUP by TdT enzyme at 37ºC for 2 hours. BrdU labeled cells were stained with anti-BrdU antibody and color developed with peroxidase substrate DAB, followed Hematoxylin counterstain.

Nutlin-3a treatment of tumor cells in culture

EL4 or B16F1 tumor cells were cultured in DMEM medium supplemented with 10% of FBS in the presence of varying concentration of nutlin-3a for different duration. Culture

supernatant was harvested for determining HMGB1 and ATP. The tumor cell apoptosis was examined via FACS analysis of 7-AAD$^+$ cells.

Western Blotting

Fifteen μl of culture supernatant from nutlin-3a treated cells was mixed with 4X LDS sample loading buffer (Invitrogen), reducing agent, and heated to 70°C for 10 minutes. Proteins were separated with NuPAGE® 10 % Bis-Tris gels (Invitrogen) and transferred onto PVDF membranes (Invitrogen). The membranes were blotted with antibodies against HMGB1 (Abcam), followed by a secondary antibody conjugated with horseradish peroxidase (Santa Cruz Biotechnology, Santa Cruz, CA). The blots were visualized using Super Signal® West Dura Chemiluminescent substrates (Pierce Biotechnology, Rockford, IL) according to the manufacturer's instructions. Western blot digital images were obtained using Fujifilm LAS-300 Imager.

Quantification of ATP concentration

Perkin Elmer luciferase-based ATPlite 1step assay kit was employed to determine ATP concentration in supernatant of nutlin-3a treated cells according to the manufacturer's instructions. Briefly, 100 μl of supernatant was mixed with 100 μl substrate solution in a white 96-well plate with shaking at 500 rpm for 5 minutes. Luminescence was measured with a BioTek Synergy HTX microplate reader.

Bone marrow derived MDSCs and DCs and *in vitro* treatment with nutlin-3a

BM-MDSCs were derived in the presence of murine recombinant IL-6 (40 ng/ml) and GM-CSF (100 U/ml) from a 4 day-culture as previously described (4). BM-DCs were derived in the presence of murine recombinant GM-CSF (1000 U/ml) in an eight-day culture with GM-CSF replenished every 2 days (24). They were treated with varying concentrations of nutlin-3a for 24 hours and their viability, phenotype, and function were subsequently assessed.

MDSC-mediated inhibition of T cell proliferation

Naïve T cells were harvested from WT mice, purified using an EasySep Mouse T cell enrichment kit (StemCell Technology, Vancouver, CA), and labelled with CFSE (Invitrogen). These T cells were incubated with purified MDSCs at the ratio of T:MDSC of 1:2.5 or 1:5 in the presence of mouse T-activator beads (Invitrogen) for 72 hours. The CFSE dilution was examined via BD™ LSR II.

Statistical analysis

Differences between different genotypes and/or treatments were analyzed via two-tailed Student's t-test using GraphPad Prism. Therapeutic effects on tumor growth between treatment groups were analyzed using two-way ANOVA (GraphPad Prism).

Results

Local p53 activation in the EL4 TME stimulates systemic antitumor immunity and tumor regression

Nutlin-3a, a potent pharmacological p53 activator, has encountered hematological toxicity in clinical application associated with systemic delivery (14). We employed EL4 and B16 tumors, which are reported to maintain WT *p53* gene (4,25), confirmed their functional p53 pathway, and determined the effective dose of nutlin-3a in mediating p53-dependent tumor killing. As expected, nutlin-3a treatment resulted in upregulation of the p53 down-stream targets *MDM2*, *puma*, and *p21* in a dose-dependent manner in both tumors (Supplementary Fig. S1A and S1B). Moreover, at up to 20 μM, nutlin-3a induced p53-specific and dose-dependent cell death (Fig. S1C). However, significant p53-independent toxicity manifested at 50 μM or higher (Fig. S1C). Thus, nutlin-3a was capped at 20 μM in culture and 100 μl of 20 μM for intratumoral (i.t.) injection. Interestingly, injection of nutlin-3a, but not PBS, into subcutaneously (s.c.) established EL4 tumors in wild type (WT) mice induced significant tumor regressions (Fig. 1A). Among the 17 nutlin-treated mice, 7 (~40%) experienced complete tumor eradication and resisted to subsequent EL4 re-challenge (Fig. 1A), suggesting the development of antitumor immunity. Analysis of tumor draining lymph nodes (TDLN), non-tumor-draining nodes at the contralateral site to injection (cLN), and spleens revealed no major differences either in their percentage of apoptosis or cellularity between the mice treated with PBS and nutlin-3a (Fig. S2). These results suggest that local i.t. injection of nutlin-3a imposes minimal systemic toxicity. Interestingly, nutlin-3a treatment of EL4 tumors in *Rag1*^{null} mice, which lack T and B cells, appeared to be ineffective in controlling tumor progression (Fig. 1B). Immunofluorescence and histochemical staining confirmed a localized upregulation of p53 in the EL4 TME treated with nutlin-3a (Fig. S3A), associated with a similar level of confined cell death following nutlin-3a treatment in the EL4 TME of both *Rag1* ^{null} and WT mice (Fig. S3B and C). These results imply the participation of adaptive immunity in nutlin-3a-induced tumor control.

To confirm the induction of systemic immunity following i.t. injection of nutlin-3a, we tested the effects of nutlin-3a treatment in WT mice bearing two established EL4 tumors, one each in the right and left flank, with only the tumor in the right receiving nutlin-3a (Fig. 1C). To ensure a sufficient period of activated immune cells to reach and attack distal tumors, we reduced the number of inoculated EL4 cells/flank to slightly delay tumor progression. Indeed, nutlin-3a injection not only induced regression of the EL4 tumors receiving nutlin-3a, but also tumors distal to the site of injection (Fig. 1C). Flow cytometry (FACS) analysis revealed a marked increase in tumor-infiltrating TILeus-CD8 cells and their enhanced IFN-γ production in tumors received nutlin-3a and tumors distal to nutlin-3a-treatment (CL-side) compared with tumors in both flanks of PBS-treated mice (Fig. 1D). Together, these results imply that nutlin-3a-induced local p53 activation in confined area of the EL4 TME leads to marked activation of effector CD8 T cells, resulting in systemic tumor regression, eradication, and protection.

Nutlin-3a-induced p53-dependent EL4 death is necessary for activation of antitumor immunity

Because therapy-induced tumor ICD is an important component for productive activation of antitumor immunity (17,20), we investigated whether nutlin-3 induces ICD of EL4 tumor and whether it is necessary for the observed tumor control. ICD is usually characterized by three hallmarks: cell surface exposure of an endoplasmic reticulum protein calreticulin (CALR), release of nuclear protein high mobility group box 1 (HMGB1), and cellular ATP to extracellular space (17,26,27). As expected, following treatment of EL4 cells with nutlin-3a, their upregulation of surface CALR (Fig. S4), release of HMGB1 (Fig. 2A), and ATP (Fig. 2B) were observed within 24–30 hours. Extracellular HMGB1 and ATP are known to activate myeloid cells, especially dendritic cells (DCs) (26) that subsequently activate T cells, we further examined DC antigen uptake and activation *in vivo* 2 days after nutlin-3a injection to GFP expressing EL4 cells (EL4-GFP). Indeed, compared with PBS treatment, nutlin-3a greatly increased $CD11c^+$ cells in the EL4-GFP TME, revealed by both IHC and FACS (Fig. 2C). Importantly, nutlin-treatment not only induced an increase in percentage of $CD11c^+$ cells, but also their activation shown as marked increase in MHC II expression, especially among the $CD11c^+CD103^+$ DC subset. (Fig. 2C). These $CD11c^+CD103^+$ cells are crucial migratory DCs capable of cross-presenting tumor antigens to activate naïve T cells in the TME and lymphoid tissues (28,29) and their enhanced GFP-antigen uptake showing as an increased percentage of $CD11c^+CD103^+GFP^+$ cells in the TME and DTLNs in nutlin-treated mice than that of PBS control mice (Fig. 2C and D). It is noteworthy that the GFP level in the TDLN-$CD11c^+CD103^+$ cells was lower than those in TILeus-$CD11c^+CD103^+$ cells because of GFP-antigen digestion/process by those DCs during their mobilization to the TDLNs (Fig. 2D). Different from EL4 tumors that maintain functional *p53*, EL4sip53 tumors that were EL4 cells modified with *p53* inactivating shRNA, were irresponsive to nutlin treatment in WT mice (Fig. 2E). In contrast, nutlin treatment of EL4si-Scarmble, EL4 tumors modified by a scramble shRNA, led to similar tumor regression to those unmodified EL4 tumors (Fig. 2E). These results confirm that p53-dependent tumor death is required for immune activation. Collectively, these results demonstrate that p53-dependent ICD of EL4 cells in the TME following nutlin-3a treatment enhances antigen uptake and activation of DCs, especially $CD11c^+CD103^+$ migratory DCs that stimulate the activation of antitumor immunity.

Nutlin-induced productive antitumor immunity also relies on a functional p53 pathway in the tumor infiltrating leukocytes

The TME is a complex ecosystem consists of TILeus and non-hematopoietic stromal cells, all of which may actively contribute to nutlin-3a-induced tumor regression. To clarify whether a functional p53 pathway in any cellular subsets other than tumor is also essential for nutlin-induced antitumor immunity, we treated EL4 tumors in $p53^{null}$ mice. Interestingly, nutlin-3a was unable to control EL4 tumor progression in $p53^{null}$ mice (Fig. 3A), implying an important role of p53 activation in other cellular compartments of the TME for nutlin-induced tumor regression. Likewise, nutlin-3a also appeared to be ineffective in controlling EL4 tumors in $p53^{flox/flox}$*vav-Cre* ($p53^{Fl}$-*vav*) mice, where *p53* is inactivated in leukocytes (Fig. 3B), suggesting the crucial role of p53 activation in the TILeus. FACS analysis of EL4 tumors established a GFP-expressing transgenic (UBC-GFP) mice suggested that nutlin-3a

induced a marked increase in TILeus ($CD45^+GFP^+$) to 13.99 ± 1.54 % from 8.31 ± 0.41 % in PBS control (Fig. 3C). Notably, the changes in percentage of various TILeu-subsets in nutlin-3a-treated EL4 TME were drastically different, including more than doubled $CD8^+$ T cells, slightly and insignificantly increased $CD11b^+$ cells, contrasting to the drastically decreased $CD19^+$ B cells and modestly reduced $CD4^+$ T cells (Fig. 3D). To examine whether these differential increase or decrease in the percentage of various immune cells was reflective to their sensitivity to nutlin-3a, we treated purified lymphoid and myeloid subsets with nutlin-3a in culture. Not surprisingly, 20 μM of nutlin-3a induced rapid death of all immune subpopulations within 24 hours, including death of ≥ 95% $CD19^+$ B cells, 85% $CD8^+$, 65% $CD4^+$ T cells, ~ 50% bone marrow derived (BM)-DCs, and ~ 65% BM-myeloid derived suppressor cells (MDSCs) (Fig. S5). These data explain the observed reduction of $CD19^+$ and $CD4^+$ cells in the nutlin-treated EL4 TME (Fig. 3D) and agree with the clinical reports of nutlin-3a-associated hematological toxicity (14). Moreover, they also imply that the observed increase in the percentages of $CD8^+$, $CD11b^+$ (Figs. 1D and 3D), and $CD11c^+$ cells (Fig. 2C) represent active processes associated with nutlin-induced immune activation.

Among $CD11b^+$ cells in the TME and tumor draining lymph nodes (TDLNs), $CD11b^+Gr\text{-}1^+$ MDSCs and activated DCs exemplify functional opposing myeloid subpopulations (28,30,31). Reduction in MDSC frequency alters immunosuppressive TME and subsequently promotes antitumor immunity. Indeed, in nutlin-3a-treated EL4 TME and TDLNs of WT mice, a marked reduction in total MDSCs, including $Ly6G^{hi}$ G-MDSCs and $Ly6C^{hi}$ M-MDSCs, was observed (Fig. S6 and Fig. 3E). Of note, the reduction of TILeu-MDSC was less profound than that in the TDLNs, likely due to compartmentalization and heterogeneity of nutlin-3a-induced local p53 activation in the TME and confined dying cells (Fig. S3).

To determine whether nutlin-3a also alters the phenotype and function of MDSCs that survive the treatment, we analyzed BM-MDSCs in culture. Similar to *in vivo* observation, nutlin-3a induced a dose-dependent reduction in G-MDSCs within 24 hours (Fig. 4A), with a concomitant increase in $CD11c^+CD80^+$ MDSCs (Fig. 4B). Early studies demonstrated that that MDSCs can be converted to DC-like myeloid populations under certain situations (32,33), we further examined their immunosuppressive capacity and revealed that these nutlin-treated “MDSCs” lost their ability to suppress the proliferation of CD4 and CD8 T cells (Fig. 4C and D). Furthermore, we harvested TIL-MDSCs from PBS and nutlin-3a treated EL4 cells in WT mice 4 days after the last i.t. injection and purified G-MDSC and M-MDSC via FACSorting (Fig. 4E). Functional analysis also confirmed that their immunosuppressive capacity of inhibiting T cell proliferation was marked reduced in nutlin-3a-treated tumors (Fig. 4E). Collectively, these results suggest that the drastic increase in the percentage of $CD8^+$ T and modest elevation of $CD11b^+$ myeloid subsets in nutlin-treated EL4 TME represent active events secondary to p53-dependent reversal of immunosuppression via functional elimination of immunosuppressive MDSCs.

Nutlin-3a induces immunogenic cell death of B16 melanomas, but is unable to control B16 progression in WT mice

Experimentally and clinically, some tumors, such as EL4, are more responsive to immunotherapy maneuvers, which are termed as immunogenic, whereas others, such as B16 melanoma, are less responsive to immunological regimens and deemed to be non-immunogenic (22,23,34). Despite *in vitro* ICD induction of B16 tumors by nutlin-3a, demonstrated as the surface exposure of CALR (Fig. S7), release of HMGB1 (Fig. 5A), and ATP (Fig. 5B) to extracellular space, nutlin-3a treatment hardly delayed B16 tumor progression *in vivo* (Fig. 5C). Because immune cell access to tumors is essential for effective tumor control (35–37), we examined leukocyte infiltration in the B16 TME. Comparative analysis of the B16 and EL4 TME revealed that the TILeus in B16 tumors were significantly lower than those of EL4 (Fig.5D). IHC staining also confirmed an overall scarce $CD3^+$ T and $CD11b^+$ myeloid cells in B16 tumors compared with those in EL4 tumors (Fig. 5E). Among TILeu-subsets, the relative composition of CD4 and CD8 cells in EL4 and B16 tumors was similar, while that of CD19 B cells was lower and that of $CD11b^+$ cells was higher in the B16 TME than those in the EL4 TME (Fig. 5F). Overall, it is postulated that the limited immune cell infiltration in the B16 TME prevents effective induction of immune activation despite nutlin-induced ICD. These results suggest that additional immunological maneuvers to markedly enhance TILeus in the B16 TME is necessary.

Ploy-IC facilities leukocyte recruitment to the B16 TME, which markedly enhances nutlin-induced antitumor immunity leading to tumor regression

Polyinosinic:polycytidilyc acid (poly-IC), a synthetic double-stranded RNA complex that mimics viral infection, has been shown to recruit and activate antigen presenting cells (APCs) via stimulating TLR3 (38,39,40). We explored the effects of poly-IC in improving immune cell recruitment to the B16 TME following i.t. injection and observed a more than 3-fold increase in total TILeus to 12.3 ±2.0 % (Fig. 6A), which peaked at 2 days and lasted for at least 6 days post-injection. We then combined poly-IC and nutlin-3a treatment by two nutlin-3a injections following a single injection of poly-IC (poly-IC + nutlin) (Fig. 6B). Remarkably, combination of poly-IC + nutlin significantly delayed B16 tumor progression (Fig. 6B), associated with large areas of tumor necrosis (Fig. 6C) and substantial immune cell infiltration (Fig. 6D). In contrast, nutlin-3a alone induced tumor cell death in confined area (Fig. 6C), which was insufficient to affect tumor progression (Fig. 6B). Although poly-IC alone greatly improved total TILeus and myeloid subpopulation (Fig. 6D), it only modestly hindered tumor progression (Fig. 6B).

Flow cytometry analysis confirmed that poly-IC and poly-IC + nutlin treatments greatly enhanced TILeus in the B16 TME (Fig. 7A). Interestingly, poly-IC alone drastically increased TILeus-$CD11b^+$ cells (Fig. S8A). TILeus-MDSC analysis suggested a similar elimination of $Ly6G^{hi}$ G-MDSC with concomitant increase in $Ly6C^{hi}$ M-MDSC-like cells in both poly-IC alone and poly-IC + nutlin treated B16 TME (Fig. 7B). Strikingly, the drastic difference between these two treatment groups was the activation status of TILeus-$CD11b^+$ cells: whereas among the one-time poly-IC-treated B16 TME, $CD11b^+$ population were dominantly $MHCII^{-/lo}$, those in the poly-IC + nutlin treated TILeus-$CD11b^+$ cells were

mostly MHCII$^{mod/hi}$ (Fig. 7C). Consequently, these activated myeloid cells in poly-IC + nutlin treated B16 TME augmented CTL activation, leading to a drastic increase in the percentage of CD8$^+$ T cells to 19.2 ± 2.7% from 9.6 ± 1.8 % in the B16 TME treated with poly-IC alone (Fig. 7D), with concomitant reduction in CD4 T cells (Fig. S8B). Remarkably, poly-IC + nultin combination further amplified effector cytokine producing CD8 cells, especially polyfunctional CTLs that produced two or more cytokines of IFN-γ, TNF-α, or IL-2 (Fig. 7E). Although poly-IC alone also improved relative frequency of polyfunctional CTLs among CD8$^+$ cells (Fig. 7E), its overall low level of CD8$^+$ T cells (Fig. 7D) dictated its modest outcome in tumor control (Fig. 6B). Together, these results demonstrate that in tumors with limited TILeus, such as B16, nutlin-induced immune activation is achievable through combinational strategy with other immunological maneuvers, such as poly-IC. These results further substantiate that p53-dependent reversal of the immunosuppressive landscape via eliminating/reversing immunosuppressive MDSCs and activating APCs is pivotal for activation of tumor-specific polyfunctional CD8 CTLs.

Discussion

This study shows that nutlin-3a-induced local p53 activation in the TME effectively promotes systemic adaptive immunity leading to tumor regression and eradication. Mechanistically, this nutlin-3a-induced productive antitumor immunity relies on two non-redundant, but synergistic processes: (1) p53-dependent tumor ICD, and (2) p53-dependent reversal of immunosuppression in the TME via functional elimination of immunosuppressive MDSCs. Specifically, tumor ICD ensures effective tumor antigen release and DC activation for antigen-specific immunity, while p53 activation in TILeus of the TME alters the dynamics and function of myeloid subpopulations for sustained T cell activation, both of which require effective T cell access to the TME for tumor elimination. Together, these two concerted events synergistically amplify nutlin-initiated confined tumor death and local immune activation to systemic antitumor immunity and tumor regression.

Recent clinical reports indicate that the conventional approach of systemic delivery of pharmacological p53 activators or re-activators are associated with hematologic toxicity (14). Our study demonstrates that local delivery of p53 activator to the TME limits its dose and toxicity and, importantly, preserves the function of immune system. Therefore, different from the conventional tumoricidal-based p53-targeted therapy that relies on effective activator delivery to reach all cancerous cells, this new strategy of exploiting the immunomodulatory function of p53 activator amplifies a localized tumor-killing process to systemic antitumor immunity with minimal toxicity. It is noteworthy that this approach is not limited to tumors maintaining WT *p53*. With clinically tested pharmacological p53 activators to targeted activate/re-activate the p53 pathway in tumors incurring WT or mutant *p53* (3,10), respectively, the application of these p53 pharmacological activators can be redirected for local use as immunotherapy regimens for enhancing antitumor immunity and broader application for combinational therapies.

Experimentally and clinically, MDSCs are one of the crucial populations in enforcing immunosuppression in the TME (30,41–43). Our study shows that activation of the p53 pathway can be exploited as a new means of eliminating MDSCs, by promoting death and/or

functional reversal of their immunosuppressive capacity. Importantly, it appears that in both El4 and B16 tumor models, p53-dependent MDSC elimination and induction of tumor ICD are essential and not interchangeable for productive activation of antitumor immunity. Although tumor ICD-mediated ATP and HMGB1 release induces DC and immune activation (17,44), this local and temporal DC activation appears to be insufficient to overcome the dominate immunosuppression in the absence of MDSC elimination, such as the EL4 TME in $p53^{null}$ mice and B16 TME in WT mice. Nevertheless, nutlin-mediated MDSC elimination/reversal in the TME and TDLNs provides a sustainable environment to amplify ICD-induced immune activation and promote the drastic expansion of polyfunctional CTLs. Likewise, in the absence of tumor ICD, such as nutlin-3a treatment of EL4sip53 tumors in WT mice, MDSC elimination/reversal in the TME was not sufficient to induce tumor antigen-specific immunity. The synergistic effects of tumor ICD and reversal of immunosuppression are further supported by the observation in B16 tumor model because nutlin-3a + poly-IC treatment in the B16 TEM simultaneously induces both events leading activation of productive antitumor immunity. On the other hand, either nutlin-3a alone, which only induced tumor ICD, or poly-IC alone, which was insufficient to overcome immunosuppression unless administrated repetitively and combining with checkpoint blockade (39,45), did not result in sustained productive antitumor immunity for tumor control.

It is also imperative to point out the significant difference between murine and human cells in p53-mediated regulation and amplification of TLR3 signaling pathway. While human cancers or immune cells modify their expression of various TLRs, including TLR3, following p53 activation (46,47), murine tumors or immune cells do not appear to alter their TLR3 expression following nutlin-3-mediated p53 activation in our studies. Thus, we postulated that clinically, the therapeutic effects of poly-IC + nutlin-3a combination might be further heightened due to p53-activation-induced upregulation of TLR3 expression in human tissues and subsequent amplification of immune activation.

Together, our study underscores the importance of p53 activity in various compartments of the TME in synergistically promoting systemic antitumor immunity. Therefore, conventional p53-activation approaches for tumoricidal effects can be repurposed for immunotherapy strategy to promote tumor antigen-specific, systemic, and durable antitumor immunity.

Supplementary Material

Refer to Web version on PubMed Central for supplementary material.

Acknowledgments

Financial support: This study is supported in part by 01CA169133 from NCI/NIH and funds from GRU Cancer Center to Y. Cui, R01CA157303 from NCI/NIH and funds from Georgia Research Alliance to E. Celis.

We would like to thank Drs. David Munn and Gang Zhou for constructive suggestions, Mr. Hussein Sultan for critical reagents, and Drs. Sumin Lu and Shuzhong Zhang for technical assistance.

References

1. Levine AJ. p53, the cellular gatekeeper for growth and division. Cell. 1997; 88(3):323–31. [PubMed: 9039259]
2. Olivier M, Hollstein M, Hainaut P. TP53 mutations in human cancers: origins, consequences, and clinical use. Cold Spring Harbor perspectives in biology. 2010; 2(1):a001008. [PubMed: 20182602]
3. Vazquez A, Bond EE, Levine AJ, Bond GL. The genetics of the p53 pathway, apoptosis and cancer therapy. Nature reviews Drug discovery. 2008; 7(12):979–87. [PubMed: 19043449]
4. Guo G, Marrero L, Rodriguez P, Del Valle L, Ochoa A, Cui Y. Trp53 inactivation in the tumor microenvironment promotes tumor progression by expanding the immunosuppressive lymphoid-like stromal network. Cancer Res. 2013; 73(6):1668–75. [PubMed: 23319800]
5. Zhang S, Zheng M, Kibe R, Huang Y, Marrero L, Warren S, et al. Trp53 negatively regulates autoimmunity via the STAT3-Th17 axis. Faseb J. 2011; 25(7):2387–98. [PubMed: 21471252]
6. Menendez D, Shatz M, Resnick MA. Interactions between the tumor suppressor p53 and immune responses. Curr Opin Oncol. 2013; 25(1):85–92. [PubMed: 23150340]
7. Cooks T, Harris CC, Oren M. Caught in the cross fire: p53 in inflammation. Carcinogenesis. 2014; 35(8):1680–90. [PubMed: 24942866]
8. Gudkov AV, Gurova KV, Komarova EA. Inflammation and p53: A Tale of Two Stresses. Genes & cancer. 2011; 2(4):503–16. [PubMed: 21779518]
9. Schwitalla S, Ziegler PK, Horst D, Becker V, Kerle I, Begus-Nahrmann Y, et al. Loss of p53 in enterocytes generates an inflammatory microenvironment enabling invasion and lymph node metastasis of carcinogen-induced colorectal tumors. Cancer cell. 2013; 23(1):93–106. [PubMed: 23273920]
10. Khoo KH, Verma CS, Lane DP. Drugging the p53 pathway: understanding the route to clinical efficacy. Nature reviews Drug discovery. 2014; 13(3):217–36. [PubMed: 24577402]
11. Brown CJ, Lain S, Verma CS, Fersht AR, Lane DP. Awakening guardian angels: drugging the p53 pathway. Nat Rev Cancer. 2009; 9(12):862–73. [PubMed: 19935675]
12. Topalian SL, Drake CG, Pardoll DM. Immune checkpoint blockade: a common denominator approach to cancer therapy. Cancer cell. 2015; 27(4):450–61. [PubMed: 25858804]
13. Pardoll D. Cancer and the Immune System: Basic Concepts and Targets for Intervention. Semin Oncol. 2015; 42(4):523–38. [PubMed: 26320058]
14. Burgess A, Chia KM, Haupt S, Thomas D, Haupt Y, Lim E. Clinical Overview of MDM2/X-Targeted Therapies. Frontiers in oncology. 2016; 6:7. [PubMed: 26858935]
15. Xue W, Zender L, Miething C, Dickins RA, Hernando E, Krizhanovsky V, et al. Senescence and tumour clearance is triggered by p53 restoration in murine liver carcinomas. Nature. 2007; 445(7128):656–60. [PubMed: 17251933]
16. Lujambio A, Akkari L, Simon J, Grace D, Tschaharganeh DF, Bolden JE, et al. Non-cell-autonomous tumor suppression by p53. Cell. 2013; 153(2):449–60. [PubMed: 23562644]
17. Kroemer G, Galluzzi L, Kepp O, Zitvogel L. Immunogenic cell death in cancer therapy. Annu Rev Immunol. 2013; 31:51–72. [PubMed: 23157435]
18. Zitvogel L, Galluzzi L, Smyth MJ, Kroemer G. Mechanism of action of conventional and targeted anticancer therapies: reinstating immunosurveillance. Immunity. 2013; 39(1):74–88. [PubMed: 23890065]
19. Formenti SC, Demaria S. Combining radiotherapy and cancer immunotherapy: a paradigm shift. Journal of the National Cancer Institute. 2013; 105(4):256–65. [PubMed: 23291374]
20. Galluzzi L, Buque A, Kepp O, Zitvogel L, Kroemer G. Immunological Effects of Conventional Chemotherapy and Targeted Anticancer Agents. Cancer cell. 2015; 28(6):690–714. [PubMed: 26678337]
21. Vassilev LT, Vu BT, Graves B, Carvajal D, Podlaski F, Filipovic Z, et al. In vivo activation of the p53 pathway by small-molecule antagonists of MDM2. Science. 2004; 303(5659):844–8. [PubMed: 14704432]

22. Chen L, McGowan P, Ashe S, Johnston J, Li Y, Hellstrom I, et al. Tumor immunogenicity determines the effect of B7 costimulation on T cell-mediated tumor immunity. J Exp Med. 1994; 179(2):523–32. [PubMed: 7507508]
23. Lechner MG, Karimi SS, Barry-Holson K, Angell TE, Murphy KA, Church CH, et al. Immunogenicity of murine solid tumor models as a defining feature of in vivo behavior and response to immunotherapy. J Immunother. 2013; 36(9):477–89. [PubMed: 24145359]
24. Cui Y, Kelleher E, Straley E, Fuchs E, Gorski K, Levitsky H, et al. Immunotherapy of established tumors using bone marrow transplantation with antigen gene--modified hematopoietic stem cells. Nat Med. 2003; 9(7):952–8. [PubMed: 12778137]
25. Hong M, Lai MD, Lin YS, Lai MZ. Antagonism of p53-dependent apoptosis by mitogen signals. Cancer Res. 1999; 59(12):2847–52. [PubMed: 10383145]
26. Apetoh L, Ghiringhelli F, Tesniere A, Criollo A, Ortiz C, Lidereau R, et al. The interaction between HMGB1 and TLR4 dictates the outcome of anticancer chemotherapy and radiotherapy. Immunol Rev. 2007; 220:47–59. [PubMed: 17979839]
27. Yamazaki T, Hannani D, Poirier-Colame V, Ladoire S, Locher C, Sistigu A, et al. Defective immunogenic cell death of HMGB1-deficient tumors: compensatory therapy with TLR4 agonists. Cell death and differentiation. 2014; 21(1):69–78. [PubMed: 23811849]
28. Broz ML, Binnewies M, Boldajipour B, Nelson AE, Pollack JL, Erle DJ, et al. Dissecting the tumor myeloid compartment reveals rare activating antigen-presenting cells critical for T cell immunity. Cancer cell. 2014; 26(5):638–52. [PubMed: 25446897]
29. Roberts EW, Broz ML, Binnewies M, Headley MB, Nelson AE, Wolf DM, et al. Critical Role for CD103+/CD141+ Dendritic Cells Bearing CCR7 for Tumor Antigen Trafficking and Priming of T Cell Immunity in Melanoma. Cancer cell. 2016
30. Gabrilovich DI, Ostrand-Rosenberg S, Bronte V. Coordinated regulation of myeloid cells by tumours. Nat Rev Immunol. 2012; 12(4):253–68. [PubMed: 22437938]
31. Ostrand-Rosenberg S, Sinha P. Myeloid-derived suppressor cells: linking inflammation and cancer. J Immunol. 2009; 182(8):4499–506. [PubMed: 19342621]
32. Thevenot PT, Sierra RA, Raber PL, Al-Khami AA, Trillo-Tinoco J, Zarreii P, et al. The stress-response sensor chop regulates the function and accumulation of myeloid-derived suppressor cells in tumors. Immunity. 2014; 41(3):389–401. [PubMed: 25238096]
33. Cubillos-Ruiz JR, Mohamed E, Rodriguez PC. Unfolding anti-tumor immunity: ER stress responses sculpt tolerogenic myeloid cells in cancer. J Immunother Cancer. 2017; 5:5. [PubMed: 28105371]
34. Schreiber TH, Raez L, Rosenblatt JD, Podack ER. Tumor immunogenicity and responsiveness to cancer vaccine therapy: the state of the art. Semin Immunol. 2010; 22(3):105–12. [PubMed: 20226686]
35. Joyce JA, Fearon DT. T cell exclusion, immune privilege, and the tumor microenvironment. Science. 2015; 348(6230):74–80. [PubMed: 25838376]
36. Gajewski TF, Woo SR, Zha Y, Spaapen R, Zheng Y, Corrales L, et al. Cancer immunotherapy strategies based on overcoming barriers within the tumor microenvironment. Curr Opin Immunol. 2013; 25(2):268–76. [PubMed: 23579075]
37. Peske JD, Thompson ED, Gemta L, Baylis RA, Fu YX, Engelhard VH. Effector lymphocyte-induced lymph node-like vasculature enables naive T-cell entry into tumours and enhanced anti-tumour immunity. Nat Commun. 2015; 6:7114. [PubMed: 25968334]
38. Salazar AM, Erlich RB, Mark A, Bhardwaj N, Herberman RB. Therapeutic in situ autovaccination against solid cancers with intratumoral poly-ICLC: case report, hypothesis, and clinical trial. Cancer Immunol Res. 2014; 2(8):720–4. [PubMed: 24801836]
39. Takemura R, Takaki H, Okada S, Shime H, Akazawa T, Oshiumi H, et al. PolyI:C-Induced, TLR3/RIP3-Dependent Necroptosis Backs Up Immune Effector-Mediated Tumor Elimination In Vivo. Cancer Immunol Res. 2015; 3(8):902–14. [PubMed: 25898986]
40. Zhu X, Nishimura F, Sasaki K, Fujita M, Dusak JE, Eguchi J, et al. Toll like receptor-3 ligand poly-ICLC promotes the efficacy of peripheral vaccinations with tumor antigen-derived peptide epitopes in murine CNS tumor models. J Transl Med. 2007; 5:10. [PubMed: 17295916]

41. Marvel D, Gabrilovich DI. Myeloid-derived suppressor cells in the tumor microenvironment: expect the unexpected. J Clin Invest. 2015; 125(9):3356–64. [PubMed: 26168215]

42. Pitt JM, Marabelle A, Eggermont A, Soria JC, Kroemer G, Zitvogel L. Targeting the tumor microenvironment: removing obstruction to anticancer immune responses and immunotherapy. Ann Oncol. 2016; 27(8):1482–92. [PubMed: 27069014]

43. Gabrilovich DI, Nagaraj S. Myeloid-derived suppressor cells as regulators of the immune system. Nat Rev Immunol. 2009; 9(3):162–74. [PubMed: 19197294]

44. Ma Y, Adjemian S, Mattarollo SR, Yamazaki T, Aymeric L, Yang H, et al. Anticancer chemotherapy-induced intratumoral recruitment and differentiation of antigen-presenting cells. Immunity. 2013; 38(4):729–41. [PubMed: 23562161]

45. Sanchez-Paulete AR, Cueto FJ, Martinez-Lopez M, Labiano S, Morales-Kastresana A, Rodriguez-Ruiz ME, et al. Cancer Immunotherapy with Immunomodulatory Anti-CD137 and Anti-PD-1 Monoclonal Antibodies Requires BATF3-Dependent Dendritic Cells. Cancer Discov. 2016; 6(1): 71–9. [PubMed: 26493961]

46. Menendez D, Lowe JM, Snipe J, Resnick MA. Ligand dependent restoration of human TLR3 signaling and death in p53 mutant cells. Oncotarget. 2016

47. Shatz M, Menendez D, Resnick MA. The human TLR innate immune gene family is differentially influenced by DNA stress and p53 status in cancer cells. Cancer Res. 2012; 72(16):3948–57. [PubMed: 22673234]

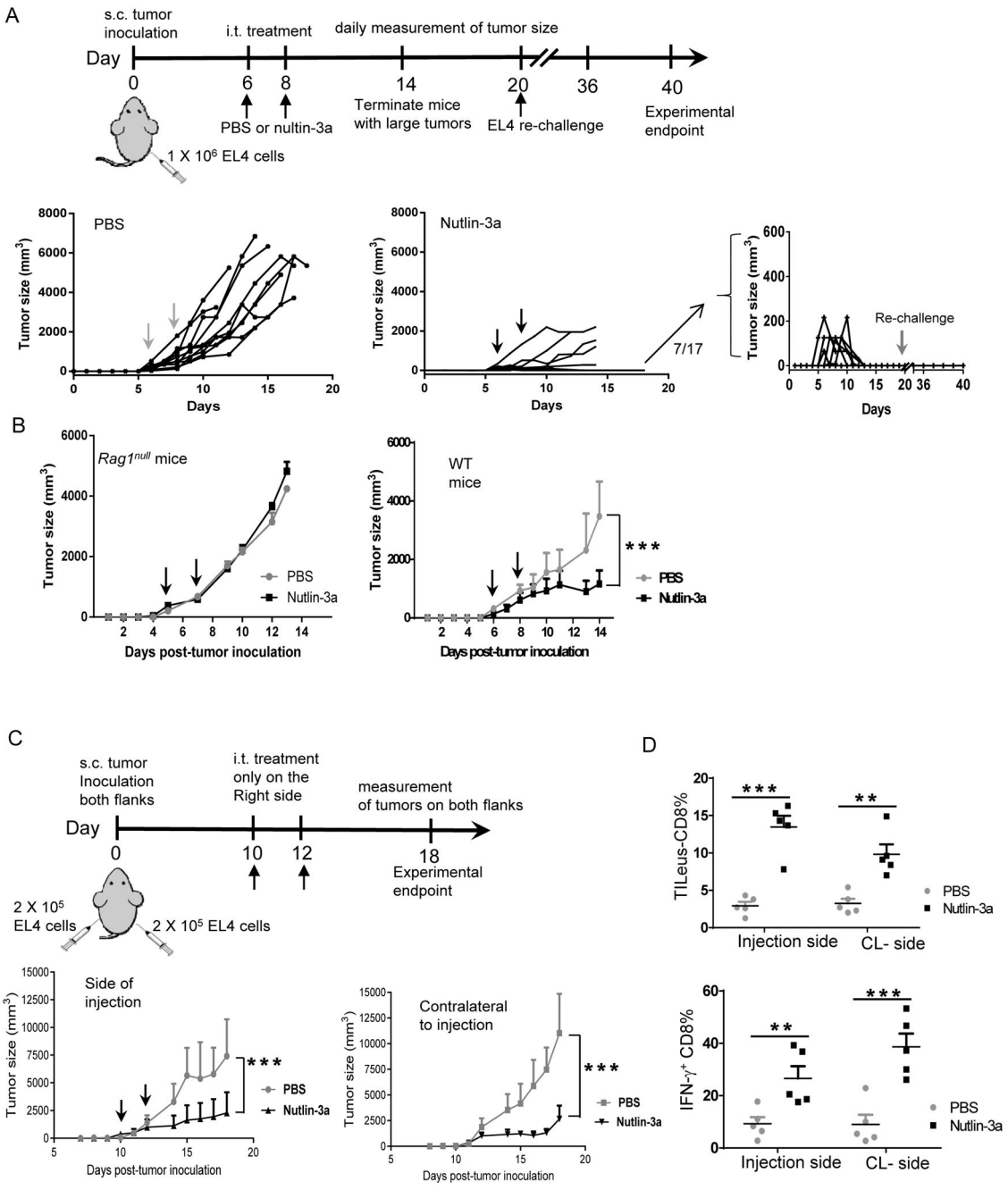

Fig. 1. Local p53 activation in the EL4 TME promotes systemic antitumor immunity and tumor regression

A. 1 X 10^6 EL4 tumor cells were injected s.c. in the right flank of WT mice. When tumors reached 100 – 300 mm^3, they were treated i.t. with 100 μl of 20 μM nutlin-3a or PBS twice, usually on day 6 and day 8. Tumor size was measured every day. When tumor diameters exceeded 15 mm, tumor bearing mice were euthanized. Nutlin-3a treated mice that experienced complete tumor elimination were re-challenged with1 X 10^6 EL4 cells on day 20. Tumor growth was assessed every other day till day 40. Individual EL4 tumor growth in WT mice treated with either PBS (left) or nutlin-3a (center and right) was plotted (n = 17–

20). **B.** EL4 tumor growth in *Rag1*^{null} and WT mice that were established s.c. and treated i.t. with 100 μl of 20 μM nutlin-3a or PBS (n = 5). **C & D.** 2 X 10^5 EL4 tumor cells were injected s.c. in both the right and left flanks of WT mice. When tumors reached 100 – 300 mm^3, usually in 10 days, tumors only in the right flank received i.t. treatment of 100 μl of 20 μM nutlin-3a or PBS twice, one day apart. **C.** Tumors in both flanks were measured every day. The size of tumor at the side of treatment (top panel) and side contralateral to the treatment (right panel) was plotted. (n = 5). **D.** The percentages of tumor infiltrating (TILeus) CD8 T cells (left panel) and IFN-γ producing CD8 cells (right panel) were determined via flow cytometry. (n =5). The experiments were repeated at least 2–3 times with similar results. Data are presented as mean ± SEM of 5 – 20 mice. **B** and **C**. *** $p < 0.001$, two-way ANOVA; D. ** $p < 0.01$, *** $p < 0.001$, two-sided Student's t-test.

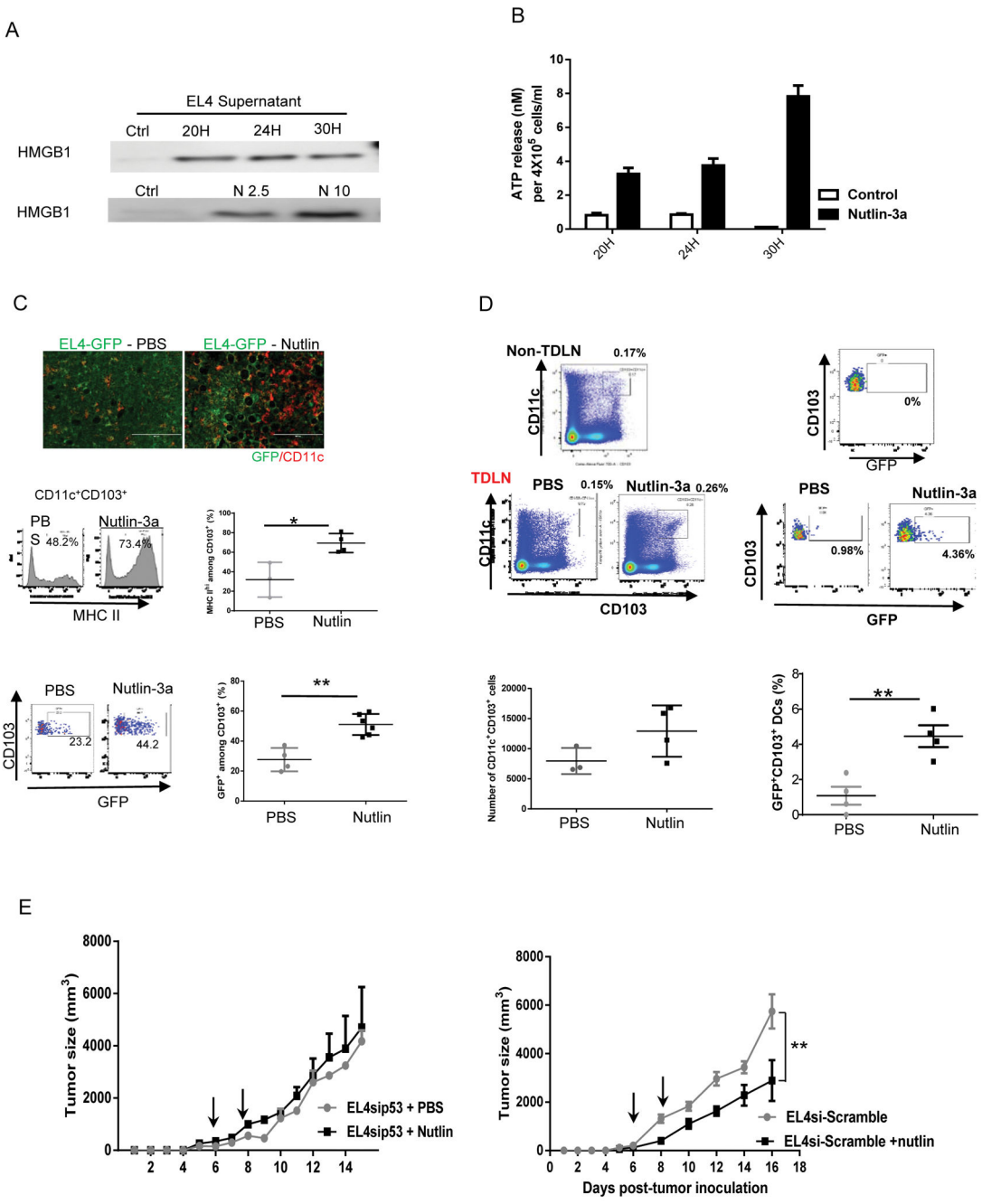

Fig. 2. Nutlin-3a-induced p53-dependent EL4 death is required for activation of antitumor immunity

A and **B.** EL4 cells were cultured in the presence of varying concentration of nutlin-3a and supernatant was harvested at 20, 24, and 30 hours post-treatment. **A.** Western blotting examination of HMGB1 release following 10 μM nutlin-3a treatment at various times (top) and various concentration of nutlin-3a at 30 hours post-treatment. **B.** Extracellular release of ATP following 10 μM of nutlin-3a treatment at various times was determined via ATPLite assay. **C.** and **D.** GFP expressing EL4 tumors (EL4-GFP) were established s.c. in WT mice and treated with PBS or 20 μM of nutlin-3a. **C**. Two days post-treatment, tumors were

harvested and processed for immunofluorescence staining of CD11c (top panel) and flow cytometry analyses of MHC II expression (middle panel) and the percentage of GFP^+ cells among $CD11c^+CD103^+$ dendritic cells (bottom panel). **D.** TDLNs from treated EL4-GFP tumors were analyzed for $CD11c^+CD103^+$ dendritic cells and GFP expression among them, using LNs from the contralateral side as non-TDLN control. The total number of TDLN-$CD11c^+CD103^+$ cells and the percentage of GFP+ cells were summarized. **E.** EL4 derivatives, EL4sip53, transduced with a lentiviral vector carrying p53shRNA, or EL4-si-Scramble, with a lentiviral vector carrying Scramble shRNA, were established s.c. in WT mice and treated with nutlin or PBS as described previously. Tumor size was measured every other day. (n = 5). The experiments were repeated at least 2–3 times with similar results. Data are presented as mean ± SEM. n = 3–6. The p value from statistical analysis is presented above each graph. **C**. and **D**. * $p < 0.05$, ** $p < 0.01$, Student's t-test. **E**. ** $p < 0.01$, two-way ANOVA.

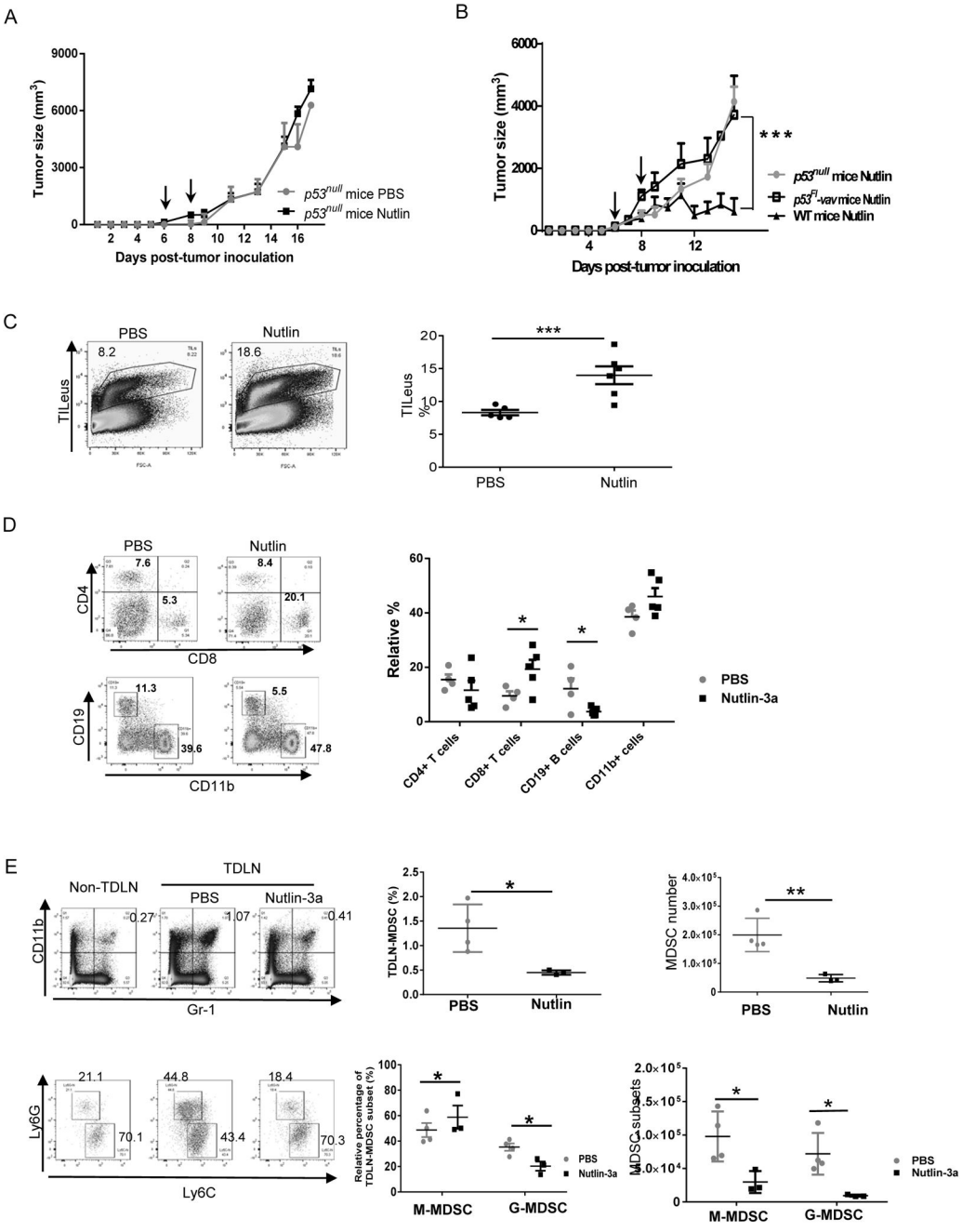

Fig. 3. Nutlin-induced activation of antitumor immunity also relies on an intact p53 pathway in the leukocytes of the TME

A. EL4 tumors were established s.c. in *p53*^{null} mice and treated with nutlin-3a or PBS twice, one day apart. Tumor size was measured every day. (n = 5) **B.** EL4 tumors established s.c. in WT, *p53*^{null}, and *p53Fl-Vav* mice were treated with nutlin-3a or PBS twice. Tumor size was measured every other day. (n = 5). **C** to **E.** EL4 tumors established s.c. in WT mice were treated with nutlin-3a or PBS twice. Six days after the last treatment, tumors and TDLNs were harvested for FACS analysis of total TILeus (**C**) and the composition of immune cell subsets in the PBS- and nutlin-treated tumors (**D**). **E**. The percentages of $CD11b^{+}Gr\text{-}1^{+}$

MDSCs and Ly6C^{hi} M-MDSCs vs. Ly6G^{hi} G-MDSCs and their absolute numbers in the TDLNs were analyzed and compared to those from non-TDLNs of the same animal. Representative FACS plots (left panel) and summary of TDLN-MDSC subsets in the PBS and nutlin-treated mice. **B**. *** $p < 0.001$, two-way ANOVA; **C** to **E.** * $p < 0.05$, ** $p < 0.01$, *** $p < 0.001$, two-sided Student's t-test.

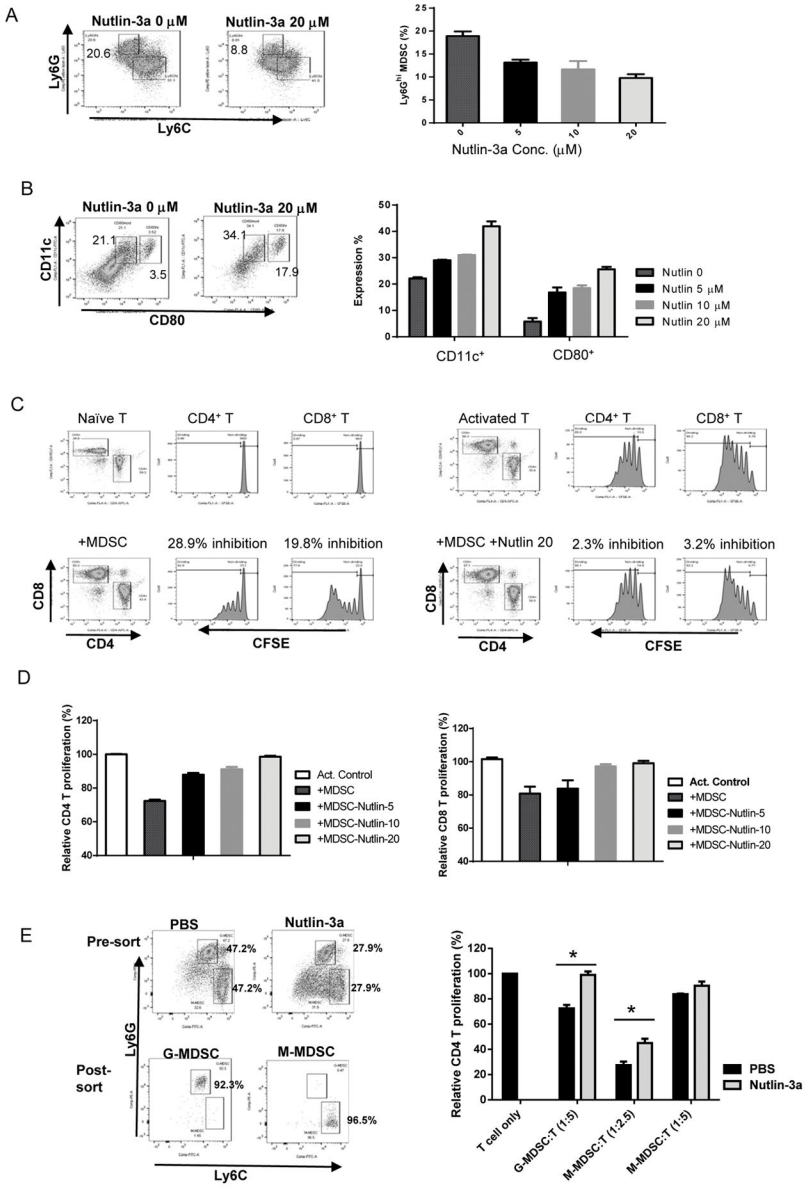

Fig. 4. Nutlin-3a reveres immune suppression by alleviating the immunosuppressive function of MDSCs

BM-MDSCs were cultured in the presence of various doses of nutlin-3a for 24 hours. $Ly6G^{hi}$ G-MDSC and $Ly6C^{hi}$ M-MDSC composition (**A**) and the percentage of $CD11c^{+}$ and $CD80^{+}$ populations among the remaining cells (**B**) was determined via flow cytometry. n = 3. **C**. The immunosuppressive ability of nutlin-treated MDSCs was evaluated via T cell proliferation assay. Representative FACS plots of CFSE labeled naïve CD4 T cells and T cells activated by anti-CD3/CD28 beads. The difference in CFSE levels between naïve and activated T cells were set as relative proliferation of 100%. **D**. Summary of dose-dependent effects of nutlin-mediated alleviation of MDSC suppression on CD4 and CD8 T cell proliferation were shown. **E.** Tumor infiltrating G-MDSCs and M-MDSCs in PBS or nutlin-3a-treated WT mice were purified via FACSorting. The effects of these purified

MDSCs on T proliferation of activation CD4 T cells were examined and summarized. Representative results of at least three independent experiments. Data are presented as mean ± SEM. n = 3–6. Experiments were repeated at least 3 times with similar results.

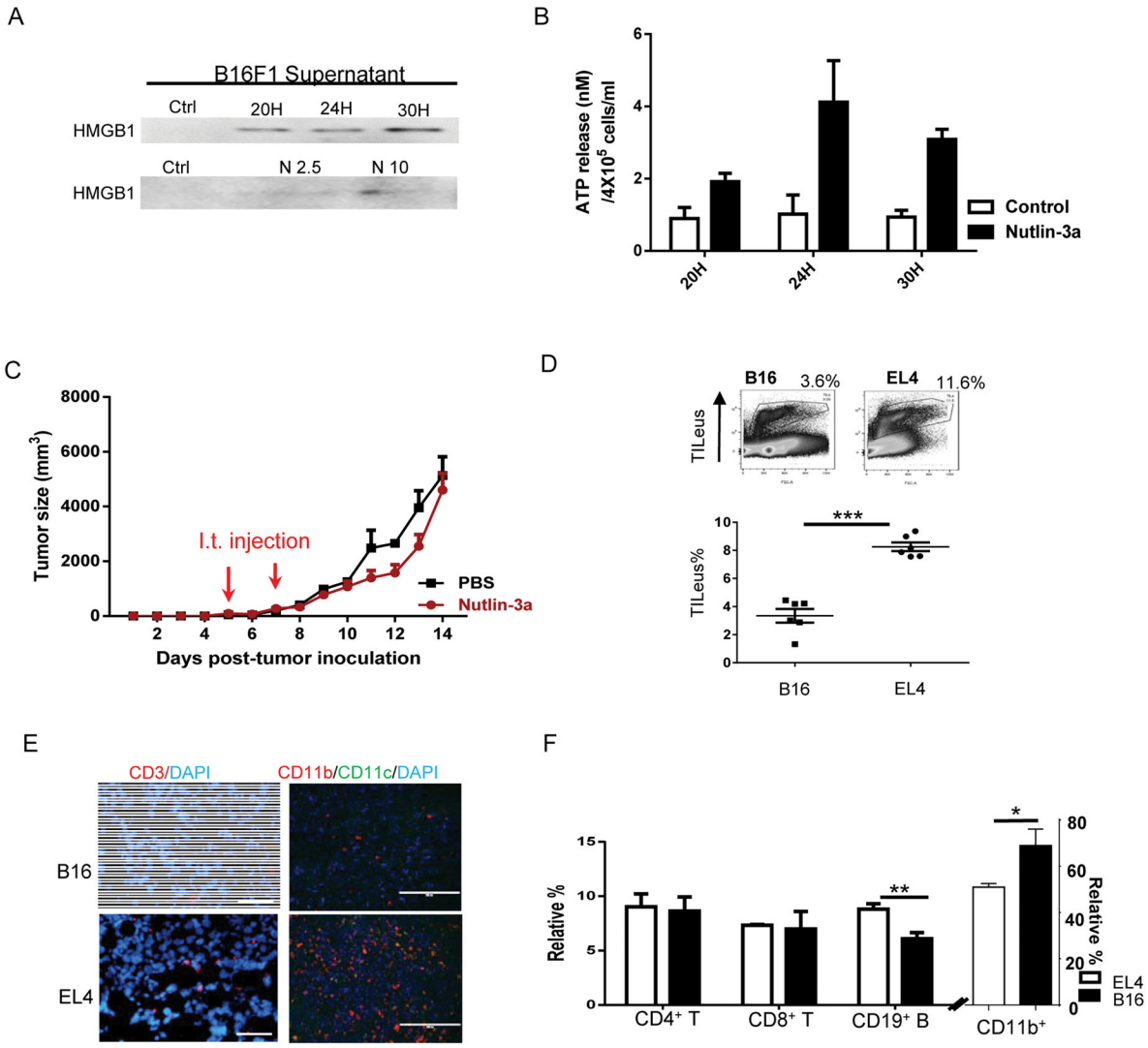

Fig. 5. Nutlin-3a induces immunogenic cell death of B16 melanomas but is unable to control B16 progression in WT mice

A and **B.** B16 melanoma cells were treated with various concentrations of nutlin-3a and supernatant was harvested at 20, 24, and 30 hours post-treatment for Western blotting examination of HMGB1 (**A**) and ATP release via ATPLite assay (**B**) following 10 μM of nutlin-3a treatment. **C.** 1 X 10^6 of B16 tumor cells were established s.c. in WT mice. When tumors reached 100 – 300 mm^3, they were treated i.t. with 100 μl of 20 μM nutlin-3a or PBS twice, one day apart. Tumor size was measured every day. (n = 10). **D to F**. EL4 and B16 were established s.c. in WT mice. When both EL4 and B16 tumors reach ~ 4000 mm^3, they were harvested. **D.** The total percentage of TILeus was examined via FACS. **E.** The abundance and distribution of TILeu-$CD3^+$ T cells and $CD11b^+$ myeloid cells was examined via IHC. **F**. The immune cell subset composition and relative percentage was analyzed via FACS. (n=5). Data are presented as mean ± SEM. Experiments were repeated at least 3 times with similar results. **D** and **F.** * $p < 0.05$, ** $p < 0.01$, *** $p < 0.001$, Student's t-test.

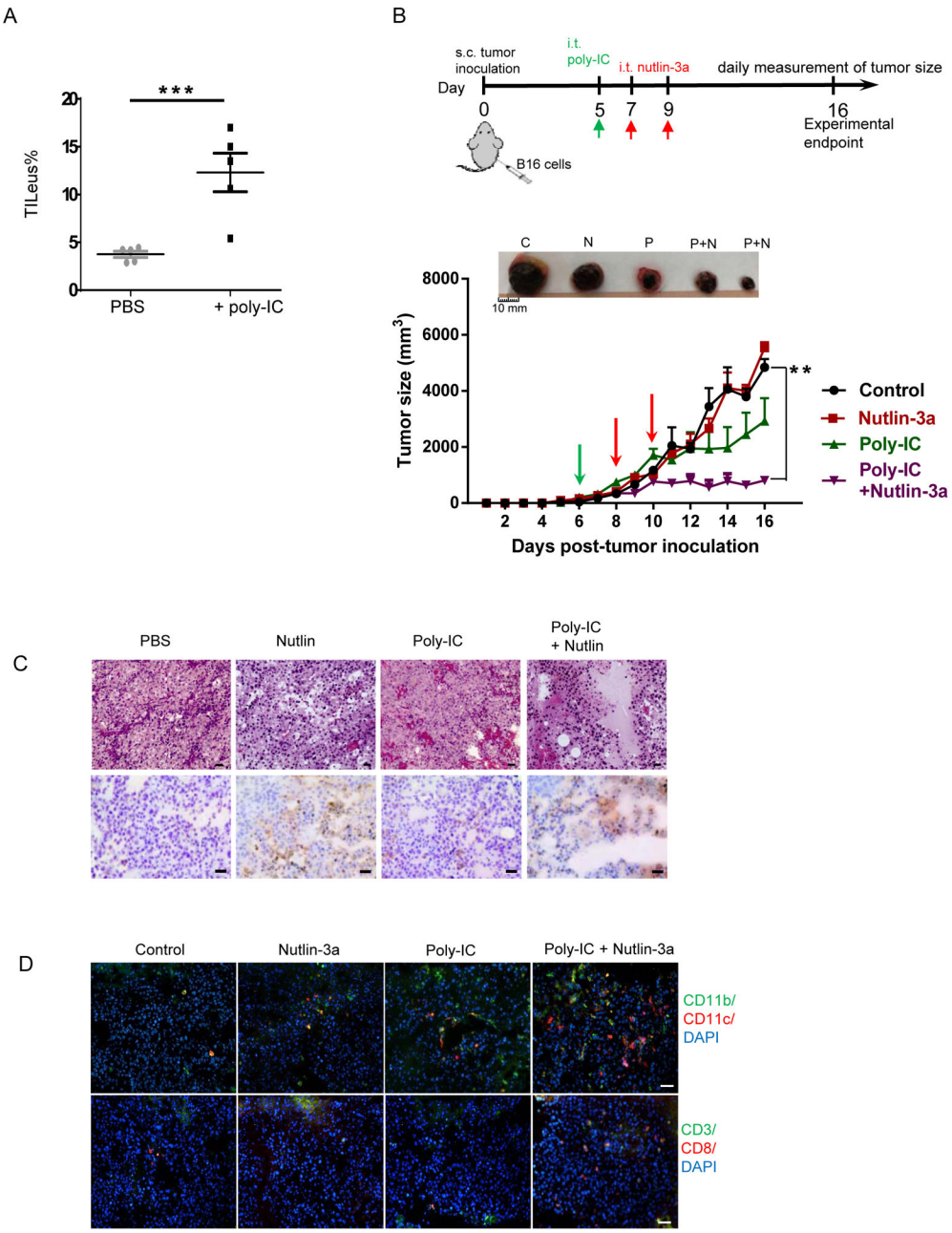

Fig. 6. Poly-IC enhances leukocyte recruitment to the B16 TME and amplifies the nutlin-3a-induced tumor cell death leading to significant tumor regression

A. B16 tumors established s.c. in WT mice were treated i.t. with 50 μg of poly-ICLC in 50 μl PBS or PBS alone as a control. Two days post-treatment, TILeus were examined via FACS. **B** to **D.** B16 tumors established s.c. in WT mice were treated i.t. with 50 μg of poly-ICLC in 50 μl PBS or PBS when tumors reached 100 – 300 mm^3. Two days later, nutlin-3a or PBS was injected i.t. twice, one day apart. **B**. The size of B16 tumors in various treatment groups were measured every day. (n = 10 – 20). Representative images of tumor size comparison at the end of the experiment (top, C = control, N = nutlin-3a, P = Poly-IC, P+N = poly-IC + nutlin-3a). **C.** Representative B16 histology analysis (H&E, top) and TUNEL

staining of dying cells (bottom) in different treatment groups. Scale bars = 50 μm. **D.** Representative images of immunofluorescence staining of TILeu-CD11b^{+} myeloid cells, CD3^{+} and CD8^{+} T cells. Scale bars = 50 μm. **B**. ** $p < 0.01$, two-way ANOVA.

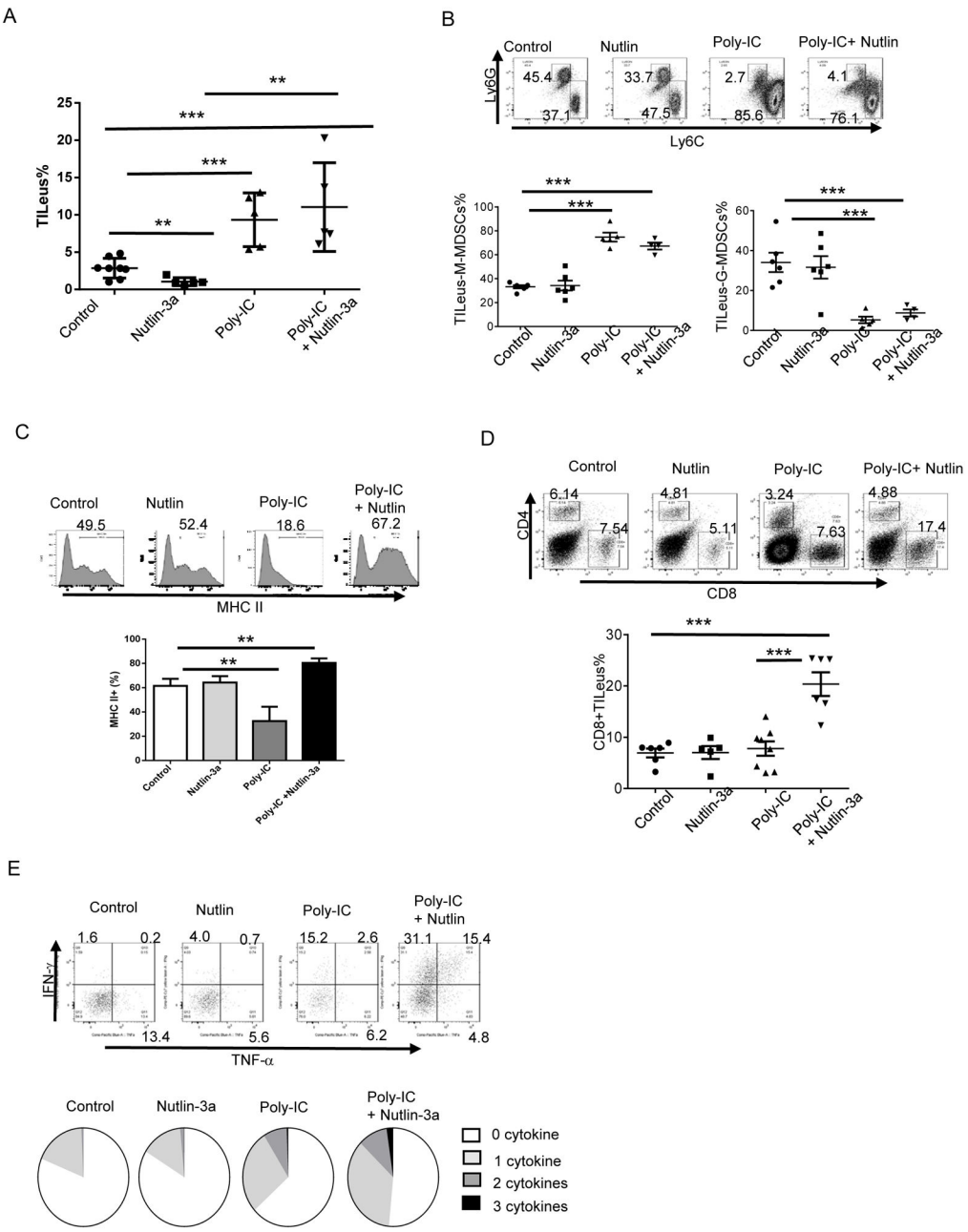

Fig. 7. Synergistic effects of poly-IC and nutlin-3a in B16 treatment are mediated through reversing immunosuppression and augmenting polyfunctional CTLs in the TME

B16 tumors established s.c. in WT mice were first treated i.t. with poly-IC or PBS, followed with nutlin-3a or PBS. At 16 days post-tumor inoculation, mice were euthanized and immune cell composition, activation status, and effector function among all treatment groups of the B16 TME were analyzed. **A**. TILeus were examined via FACS. **B.** MDSC subset composition of M-MDSCs and G-MDSCs in different treatment groups was examined via FACS. **C**. MHC II^+ cell percentage and relative MHC II expression among $CD11b^+$ myeloid cells in different treatment groups were determined via FACS. **D**. TILeus-CD8 and CD4 T cell composition in different treatment group of the B16 TME was determined via FACS. **E.**

Effector cytokine producing TILeu-CD8$^+$ T cells were determined via FACS following intracellular staining and presented in pie chart showing the composition of cytokine producing cells among total TILeu-CD8 cells. Data are presented as mean ± SEM. n = 3–6. Experiments were repeated 2–3 times with similar results. ** $p < 0.01$, *** $p < 0.001$, Student's t-test.